

1 PREPARED FOR SUBMISSION TO JHEP

## 2 Next-to-leading-order QCD corrections to the yields 3 and polarisations of $J/\psi$ and $\Upsilon$ directly produced in 4 association with a $Z$ boson at the LHC

---

5 **Bin Gong**,<sup>*a,b*</sup> **Jean-Philippe Lansberg**,<sup>*c*</sup> **Cédric Lorcé**,<sup>*c,d*</sup> **Jianxiong Wang**<sup>*a,b*</sup>

6 <sup>*a*</sup>*Institute of High Energy Physics, CAS, P.O. Box 918(4), Beijing, 100049, China*

7 <sup>*b*</sup>*Theoretical Physics Center for Science Facilities, CAS, Beijing, 100049, China*

8 <sup>*c*</sup>*IPNO, Université Paris-Sud, CNRS/IN2P3, 91406, Orsay France*

9 <sup>*d*</sup>*LPT, Université Paris-Sud, CNRS, 91406, Orsay France*

10 *E-mail:* [twain@ihep.ac.cn](mailto:twain@ihep.ac.cn), [lansberg@in2p3.fr](mailto:lansberg@in2p3.fr), [lorce@ipno.in2p3.fr](mailto:lorce@ipno.in2p3.fr),  
[jxwang@ihep.ac.cn](mailto:jxwang@ihep.ac.cn)

11 **ABSTRACT:** We update the study of the production of direct  $J/\psi$  in association with a  $Z$   
12 boson at the Next-to-Leading Order (NLO) in  $\alpha_s$  by evaluating both the yield differential  
13 in  $P_T$  and the  $J/\psi$  polarisation in the QCD-based Colour-Singlet Model (CSM). Contrary  
14 to an earlier claim, QCD corrections at small and mid  $P_T$  are small if one assumes that the  
15 factorisation and the renormalisation scales are commensurate with the  $Z$  boson mass. As it  
16 can be anticipated, the  $t$ -channel gluon-exchange ( $t$ -CGE) topologies start to be dominant  
17 only for  $P_T \gtrsim m_Z/2$ . The polarisation pattern is not altered by the QCD corrections. This  
18 is thus far the first quarkonium-production process where this is observed in the CSM.  
19 Along the same lines, our predictions for direct  $\Upsilon + Z$  are also given.

20 **KEYWORDS:**  $J/\psi$  and  $\Upsilon$  production,  $Z$  boson, QCD corrections

---

21	<b>Contents</b>	
22	<b>1 Introduction</b>	<b>1</b>
23	<b>2 Cross section at LO accuracy</b>	<b>3</b>
24	<b>3 Cross section at NLO accuracy</b>	<b>4</b>
25	3.1 Virtual corrections	4
26	3.2 Real corrections	5
27	3.3 NLO* cross section	5
28	<b>4 Results for <math>J/\psi + Z</math>: differential cross section in <math>P_T</math></b>	<b>6</b>
29	4.1 Comparison with Mao <i>et al.</i> [32]	6
30	4.2 Results for the differential cross section in $P_T$ at $\sqrt{s} = 8$ TeV and 14 TeV	8
31	4.3 Scale sensitivity at different $P_T$	10
32	<b>5 Polarisation: polar anisotropy in the helicity frame</b>	<b>11</b>
33	<b>6 Results for <math>\Upsilon + Z</math></b>	<b>12</b>
34	<b>7 Conclusions</b>	<b>14</b>

---

## 35 1 Introduction

36 A few years ago, non-perturbative effects associated with colour-octet (CO) channels [1–  
37 3] were considered to be the only plausible explanation for the numerous puzzles in the  
38 predictions of quarkonium-production rates at hadron colliders. The situation has slightly  
39 changed since then, with the first evaluations of the QCD corrections [4–8] to the yields  
40 of  $J/\psi$  and  $\Upsilon$  (commonly denoted  $\mathcal{Q}$  hereafter) produced in high-energy hadron collisions  
41 via Colour-Singlet (CS) transitions [9]. It is now indeed widely accepted [10–12] that  $\alpha_s^4$   
42 and  $\alpha_s^5$  corrections to the CSM are significantly larger than  $\alpha_s^3$  contributions at mid and  
43 large  $P_T$  and that they should be taken into account in any analysis of their  $P_T$  spectrum.  
44 Nowadays, it not clear anymore that CO channels dominate and they are the only source  
45 of quarkonia. As a result, there is no consensus on which mechanisms are effectively at  
46 work in quarkonium hadroproduction at high energies, that is at RHIC, at the Tevatron  
47 and, recently, at the LHC.

48 Polarisation predictions for the CS channel are also strongly affected by QCD correc-  
49 tions as demonstrated in [6, 8, 13, 14]. At NLO,  $\mathcal{Q}$  produced inclusively or in association  
50 with a photon are expected to be longitudinally polarised when  $P_T$  gets larger, whereas  
51 they were thought to be transversely polarised as predicted at LO in the CSM [15, 16].  
52 Such a drastic change is understood by the dominance of new production topologies. This

also explains the significant enhancement in the production rates as observed for increasing  $P_T$ .

The situation is rather different at low  $P_T$ , where the CS predictions for  $\mathcal{Q}$  at LO [9] and NLO [4–6] accuracy are of the same magnitude at RHIC energies; this shows a good convergence of the perturbative series. They are also in agreement [17–19] with the existing data from RHIC [20] energy all the way up to that of the LHC [21–28]. CO channels are most likely not needed to account for low  $P_T$  data –and thus for the  $P_T$  integrated yields. This is at odds with earlier works, *e.g.* [29], which wrongly assumed that  $\chi_c$  feed-down could be the dominant CSM contribution. This is supported further by the results of recent works [30] focusing on production at  $e^+e^-$  colliders which have posed stringent constraints on the size of  $C = +1$  CO contributions which can be involved in hadroproduction at low  $P_T$ . Finally, this is reminiscent of the broad fixed-target measurement survey of total cross sections [31] which challenged the universality of the CO MEs.

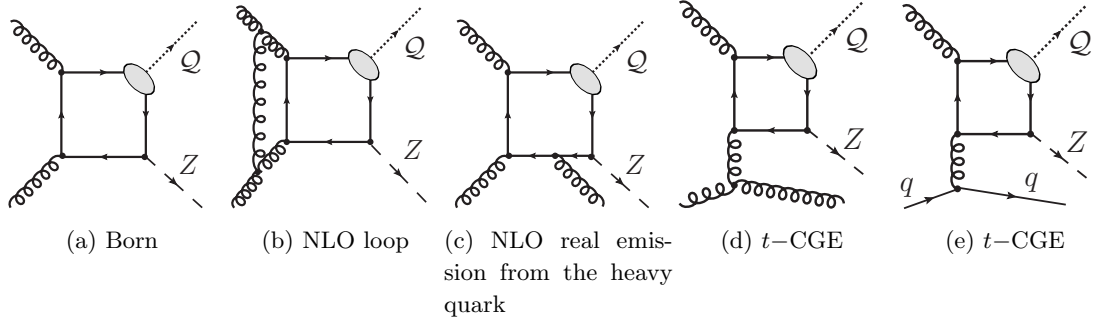


**Figure 1:** Representative diagrams contributing to  $J/\psi$  and  $\Upsilon$  (denoted  $\mathcal{Q}$ ) hadroproduction with a  $Z$  boson in the CSM by gluon fusion at orders  $\alpha\alpha_s^2$  (a),  $\alpha\alpha_s^3$  (b,c,d) and initiated by a light-quark gluon fusion at order  $\alpha\alpha_s^3$  (e). The quark and antiquark attached to the ellipsis are taken as on-shell and their relative velocity  $v$  is set to zero.

In this paper, we focus on the production of  $J/\psi$  (and  $\Upsilon$ ) in association with a  $Z$  boson. Whereas this process may give us complementary information on quarkonium production if it happens to be experimentally accessible at the LHC, it also offers an interesting theoretical playground for the understanding of the QCD corrections in quarkonium-production processes. Our motivation was twofold: first, to see if the polarisation pattern of the  $J/\psi$  is altered by the QCD corrections at large  $P_T$ ; second, to see how large the effect of new topologies opening at NLO is, by comparing a full NLO computation to a simplified one – NLO\* – with an infrared (IR) cut-off and neglecting loops. Our attention has also been drawn to this process by a previous analysis of the yield at NLO [32] which showed an intriguing result where NLO corrections were large at low  $P_T$  and getting smaller at large(r)  $P_T$ . Such a result could only be explained by a negligible contribution from new kinematically enhanced topologies and a large (positive) contribution from loop corrections at low  $P_T$ . As we shall demonstrate, the conclusion drawn in [32] are misguided by an unconventional choice of the factorisation and renormalisation scales ( $\mu_F$  and  $\mu_R$ ), –way below  $m_Z$ – and a  $P_T$  range not large enough –compared to  $m_Z$ – to be able to observe the dominance of

81  $t$ -CGE topologies. As a matter of fact, if one chooses a value for the scales commensurate  
 82 with  $m_Z$ , rather than the transverse mass of the  $J/\psi$  as done in [32], the NLO corrections  
 83 are found to be small at small  $P_T$ . On the other hand, for  $P_T \gtrsim m_Z/2$ , the NLO corrections  
 84 are enhanced by a kinematical factor  $P_T^2$ .

85 The paper is organised as follows. In sections 2 and 3, we describe the evaluation of  
 86 the cross section at LO and NLO accuracy in the CSM. We also explain how the partial  
 87 NLO\* yield is evaluated. In section 4, we present our results which we first compare to  
 88 those from [32] with the same scale choice, at the same energy and in the same kinematical  
 89 region. Then, we show our predictions in an extended  $P_T$  range for  $\mu_{F,R}$  commensurate  
 90 with  $m_Z$  and we discuss the ratio NLO over LO. We also study the sensitivity of our  
 91 prediction on the aforementioned scales. Afterward, we compare the NLO\* yield with the  
 92 full NLO and we comment on the dependence on the IR cut-off at large  $P_T$  and on the  
 93 impact of the  $t$ -CGE topologies. In section 5, we analyse the yield polarisation at LO,  
 94 NLO and NLO\*. In section 6, we give and discuss our predictions for  $\Upsilon$ . Section 7 gathers  
 95 our conclusions.

## 96 2 Cross section at LO accuracy

97 In the CSM [9], the matrix element to create a  $^3S_1$  quarkonium  $\mathcal{Q}$  with a momentum  $P_{\mathcal{Q}}$   
 98 and a polarisation  $\lambda$  accompanied by other partons, noted  $j$ , and a  $Z$  boson of momentum  
 99  $P_Z$  is the product of the amplitude to create the corresponding heavy-quark pair,  $\mathcal{M}(ab \rightarrow$   
 100  $Q\bar{Q})$ , a spin projector  $N(\lambda|s_1, s_2)$  and  $R(0)$ , the radial wave function at the origin in the  
 101 configuration space, obtained from the leptonic width, namely

$$\begin{aligned} \mathcal{M}(ab \rightarrow \mathcal{Q}^\lambda(P_{\mathcal{Q}}) + Z(p_Z) + j) &= \sum_{s_1, s_2, i, i'} \frac{N(\lambda|s_1, s_2)}{\sqrt{m_{\mathcal{Q}}}} \frac{\delta^{ii'}}{\sqrt{N_c}} \frac{R(0)}{\sqrt{4\pi}} \\ &\times \mathcal{M}(ab \rightarrow Q_i^{s_1} \bar{Q}_{i'}^{s_2}(\mathbf{p} = \mathbf{0}) + Z(p_Z) + j), \end{aligned} \quad (2.1)$$

102 where  $P_{\mathcal{Q}} = p_Q + p_{\bar{Q}}$ ,  $p = (p_Q - p_{\bar{Q}})/2$ ,  $s_1$  and  $s_2$  are the heavy-quark spins, and  $\delta^{ii'}/\sqrt{N_c}$  is  
 103 the projector onto a CS state.  $N(\lambda|s_1, s_2)$  can be written as  $\frac{\varepsilon_\mu^\lambda}{2\sqrt{2}m_{\mathcal{Q}}} \bar{v}(\frac{\mathbf{P}_{\mathcal{Q}}}{2}, s_2) \gamma^\mu u(\frac{\mathbf{P}_{\mathcal{Q}}}{2}, s_1)$  in  
 104 the non-relativistic limit with  $\varepsilon_\mu^\lambda$  being the polarisation vector of the quarkonium. Summing  
 105 over the quark spin yields to traces which can be evaluated in a standard way.

106 At LO, there is only a single partonic process at work, namely  $gg \rightarrow J/\psi Z$  –completely  
 107 analogous to  $gg \rightarrow J/\psi \gamma$  for  $J/\psi$ -prompt photon associated production– with 4 Feynman  
 108 graphs to be evaluated. One of them is drawn on Fig. 1 (a). The differential partonic cross  
 109 section is readily obtained from the amplitude squared<sup>1</sup>,

$$\frac{d\hat{\sigma}}{d\hat{t}} = \frac{1}{16\pi\hat{s}} |\mathcal{M}|^2, \quad (2.2)$$

110 from which one obtains the double differential cross section in  $P_T$  ( $P_T \equiv P_{J/\psi, T}$ ) and the  
 111  $J/\psi$  rapidity,  $y$ , for  $pp \rightarrow J/\psi Z$  after convolution with the gluon PDFs and a change of

---

<sup>1</sup>The momenta of the initial gluons,  $k_{1,2}$ , are, as usual in the parton model, related to those of the colliding hadrons ( $p_{1,2}$ ) through  $k_{1,2} = x_{1,2} p_{1,2}$ . One then defines the Mandelstam variables for the partonic system:  $\hat{s} = sx_1x_2$ ,  $\hat{t} = (k_1 - P_{J/\psi})^2$  and  $\hat{u} = (k_2 - P_{J/\psi})^2$ .

112 variable:

$$\frac{d\sigma}{dydP_T} = \int_{x_1^{\min}}^1 dx_1 \frac{2\hat{s}P_T g(x_1, \mu_F) g(x_2(x_1), \mu_F)}{\sqrt{s}(\sqrt{s}x_1 - m_T e^y)} \frac{d\hat{\sigma}}{d\hat{t}}, \quad (2.3)$$

113 where  $x_1^{\min} = \frac{m_T \sqrt{s} e^y - m_{J/\psi}^2 + m_Z^2}{\sqrt{s}(\sqrt{s} - m_T e^{-y})}$ ,  $m_T = \sqrt{m_{J/\psi}^2 + P_T^2}$ .

### 114 3 Cross section at NLO accuracy

115 The NLO contributions can be divided in two sets: one gathers the virtual corrections  
116 which arise from loop diagrams, the other gathers the real (emission) corrections where  
117 one more particle appears in the final state. In the next sections, we briefly describe how  
118 these are computed.

#### 119 3.1 Virtual corrections

120 The computation of the virtual corrections involves three types of singularities: the ul-  
121 traviolet (UV), the infrared (IR) and the Coulomb ones. UV divergences arising from  
122 self-energy and triangle diagrams are cancelled after renormalisation. A similar renormal-  
123 isation scheme as in Ref. [33] is used, except for the fact that, in the present study, the  
124 bottom quark is also included in the renormalisation of the gluon field. The renormali-  
125 sation constants  $Z_m$ ,  $Z_2$  and  $Z_3$  which are associated to the charm quark mass  $m_c$ , the  
126 charm-field  $\psi_c$  and the gluon field  $A_\mu^a$  are defined in the on-mass-shell (OS) scheme while  
127  $Z_g$ , for the QCD gauge coupling constant  $\alpha_s$  is defined in the modified minimal-subtraction  
128 ( $\overline{\text{MS}}$ ) scheme:

$$\begin{aligned} \delta Z_m^{OS} &= -3C_F \frac{\alpha_s}{4\pi} \left[ \frac{1}{\epsilon_{\text{UV}}} - \gamma_E + \ln \frac{4\pi\mu_R^2}{m_c^2} + \frac{4}{3} \right], \\ \delta Z_2^{OS} &= -C_F \frac{\alpha_s}{4\pi} \left[ \frac{1}{\epsilon_{\text{UV}}} + \frac{2}{\epsilon_{\text{IR}}} - 3\gamma_E + 3 \ln \frac{4\pi\mu_R^2}{m_c^2} + 4 \right], \\ \delta Z_3^{OS} &= \frac{\alpha_s}{4\pi} \left[ (\beta'_0 - 2C_A) \left( \frac{1}{\epsilon_{\text{UV}}} - \frac{1}{\epsilon_{\text{IR}}} \right) \right. \\ &\quad \left. - \frac{4}{3} T_F \left( \frac{1}{\epsilon_{\text{UV}}} - \gamma_E + \ln \frac{4\pi\mu_R^2}{m_c^2} \right) - \frac{4}{3} T_F \left( \frac{1}{\epsilon_{\text{UV}}} - \gamma_E + \ln \frac{4\pi\mu_R^2}{m_c^2} \right) \right], \quad (3.1) \\ \delta Z_g^{\overline{\text{MS}}} &= -\frac{\beta_0}{2} \frac{\alpha_s}{4\pi} \left[ \frac{1}{\epsilon_{\text{UV}}} - \gamma_E + \ln(4\pi) \right], \end{aligned}$$

129 where  $\gamma_E$  is Euler's constant,  $\beta_0 = \frac{11}{3}C_A - \frac{4}{3}T_F n_f$  is the one-loop coefficient of the QCD  
130 beta function and  $n_f$  is the number of active quark flavours. We take the three light quarks  
131  $u, d, s$  as massless and consider the quarks  $c$  and  $b$  as heavy; therefore  $n_f=5$ . In  $SU(3)_c$ ,  
132 we have the following colour factor:  $T_F = \frac{1}{2}$ ,  $C_F = \frac{4}{3}$ ,  $C_A = 3$ . Finally,  $\beta'_0 \equiv \beta_0 + \frac{8}{3}T_F =$   
133  $\frac{11}{3}C_A - \frac{4}{3}T_F n_{lf}$  where  $n_{lf} \equiv n_f - 2 = 3$  is the number of light quark flavours.

134 After having fixed our renormalisation scheme, there are 111 virtual-correction dia-  
135 grams, including counter-term diagrams. Diagrams that have a virtual gluon line connect-  
136 ing the charm quark pair forming the  $J/\psi$  lead to Coulomb singularity  $\sim \pi^2/|p|$ , which  
137 can be isolated and mapped into the  $c\bar{c}$  wave function.

138 The loop integration has been carried out thanks to the newly upgraded Feynman  
 139 Diagram Calculation (FDC) package [34], with the implementation of the reduction method  
 140 for loop integrals proposed in Ref. [35].

### 141 3.2 Real corrections

142 The real corrections arise from three parton level subprocesses:

$$g + g \rightarrow J/\psi + Z + g, \quad (3.2)$$

$$g + q(\bar{q}) \rightarrow J/\psi + Z + q(\bar{q}), \quad (3.3)$$

$$q + \bar{q} \rightarrow J/\psi + Z + g, \quad (3.4)$$

143 where  $q$  denotes light quarks with different flavours ( $u, d, s$ ). We have not considered the  
 144 contributions from the processes  $c\bar{c} \rightarrow J/\psi + Z + g$  and  $g + c(\bar{c}) \rightarrow J/\psi + Z + c(\bar{c})$ . Both  
 145 are IR finite and can be safely separated out from the other ones. The charm-gluon fusion  
 146 contribution may be non-negligible in the presence of intrinsic charm. It will be considered  
 147 in a separate work.

148 The contribution from the quark-antiquark fusion (Eq. (3.4)) is also IR finite and small.  
 149 The phase-space integration of the other two subprocesses will generate IR singularities,  
 150 which are either soft or collinear and which can be conveniently isolated by slicing the  
 151 phase space into different regions. We use the two-cutoff phase-space-slicing method [36],  
 152 which introduces two small cutoffs to decompose the phase space into three parts. The  
 153 real cross section can then be written as

$$\sigma^{\text{Real}} = \sigma^{\text{Soft}} + \sigma^{\text{Hard Collinear}} + \sigma^{\text{Hard Noncollinear}}. \quad (3.5)$$

154 The hard noncollinear part  $\sigma^{\text{Hard Noncollinear}}$  is IR finite and can be numerically com-  
 155 puted using standard Monte-Carlo integration techniques. Only the real subprocess of  
 156 Eq. (3.2) contains soft singularities. Collinear singularities appear in both real subpro-  
 157 cesses of Eq. (3.2) and Eq. (3.3), but only as initial-state collinear singularities. As shown  
 158 in Ref. [36], all these singularities can be factored out analytically in the corresponding  
 159 regions. When combined with the IR singularities appearing in the virtual corrections (see  
 160 section 3.1), the soft singularities of the real part cancel. Yet, some collinear singularities  
 161 remain. These are fully absorbed into the redefinition of the parton distribution function  
 162 (PDF): this is usually referred to as the mass factorisation [37]. All the singularities are  
 163 thus eventually analytically cancelled.

### 164 3.3 NLO\* cross section

165 In order to evaluate the NLO\* contributions, we use the framework described in [38] based  
 166 on the tree-level matrix-element generator MADONIA [39] slightly tuned to implement an  
 167 IR cut-off on all light parton-pair invariant mass. The LO cross section has also been  
 168 checked with MADONIA.

169 The procedure used here to evaluate the leading- $P_T$  NLO contributions is exactly the  
 170 same as in [8] but for the process  $pp \rightarrow J/\psi + Z + \text{jet}$ . Namely, the real-emission contri-  
 171 butions at  $\alpha\alpha_s^3$  are evaluated using MADONIA by imposing a lower bound on the invariant

mass of any light parton pair ( $s_{ij}^{\min}$ ). The underlying idea in the inclusive<sup>2</sup> case was that for the new channels opening up at NLO which have a leading- $P_T$  behaviour (for instance the  $t$ -CGE), the cut-off dependence should decrease for increasing  $P_T$  since no collinear or soft divergences can appear there. For other NLO channels, whose Born contribution is at LO, the cut would produce logarithms of  $s_{ij}/s_{ij}^{\min}$ , which are not necessarily negligible. Nevertheless, they can be factorised over their corresponding Born contribution, which scales as  $P_T^{-8}$ , and are thence suppressed by at least two powers of  $P_T$  with respect to the leading- $P_T$  contributions ( $P_T^{-6}$ ) at this order. The sensitivity on  $s_{ij}^{\min}$  should vanish at large  $P_T$ . This argument has been checked in the inclusive case for  $\Upsilon$  [8] and  $\psi$  [10] as well as in association with a photon [14]. Because of the presence of the  $Z$  boson mass, it is not a priori obvious that  $t$ -CGE topologies dominate over the LO ones. It is thus not clear at all how such procedure to evaluate the NLO\* yield can provide a reliable evaluation of the full NLO of  $J/\psi + Z$ . In fact, at mid  $P_T$ , significantly below the  $Z$  boson mass, the difference of the  $P_T$  dependence of the NLO and LO cross sections is maybe not large enough for the dependence on  $s_{ij}^{\min}$  to decrease fast. Having at hand a full NLO computation, we can carry out such a comparison and better investigate the effect of QCD corrections in quarkonium production. This is done after our complete results are presented.

## 4 Results for $J/\psi + Z$ : differential cross section in $P_T$

### 4.1 Comparison with Mao *et al.* [32]

In order to compare our results with those of [32], we take  $\sqrt{s} = 14$  TeV and  $|y^{J/\psi}| < 3.0$ . We also set the factorisation and renormalisation scales at the same value, namely  $\mu_F = \mu_R = m_T^{J/\psi} = \sqrt{m_{J/\psi}^2 + P_T^2}$ . We also take  $\alpha = 1/137$ ,  $|R_{J/\psi}(0)|^2 = 0.91 \text{ GeV}^3$ ,  $m_c = 1.5 \text{ GeV}$ ,  $m_z = 91.1876 \text{ GeV}$  and  $\sin^2(\theta_W) = 0.23116$ . Our LO results (also cross-checked with MADONIA) do match with those of [32] (compare both blue curves on Fig. 2).

However, as depicted in Fig. 2, we are not able to reproduce the NLO results presented in the later reference. At low  $P_T$ , we have found a  $K$  factor smaller than one (*i.e.* the yield at NLO is smaller than at LO) while they obtained a value larger than one. The way  $\alpha_s$  is precisely evaluated in both computations may differ but this can hardly explain a sign change in the  $\alpha\alpha_s^3$  contributions. There is also a difference in the renormalisation scheme: we have included both charm and bottom quarks in the renormalisation of the gluon field contrary to what has been done in the previous analysis. Yet, we do not believe that this could explain the discrepancies between both results.

That being said, a scale close to  $m_Z$ , rather than the transverse mass of the  $J/\psi$  taken in [32], seems more appropriate as done for instance for  $Z + b$ -jet [40]. This has an important effect on the scale sensitivity, less on the final numbers predicted for the yields, as we shall discuss in the next section.

In Fig. 3, we show the scale sensitivity at low  $P_T$  around two different choices of the “default” scale value,  $\mu_0$ , (a) the transverse mass of the  $J/\psi$  and (b) the  $Z$  boson mass. We

<sup>2</sup>“Inclusive” is used here in opposition to “in association with another detected particle” which is indeed a more exclusive process.

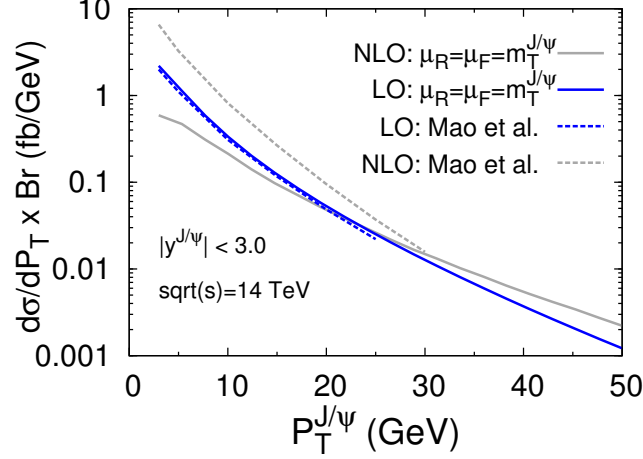


**Figure 2:** Comparison between our results (solid lines) and that of Mao et al. [32] (dashed lines) for the differential cross section for  $J/\psi + Z$  vs. the  $J/\psi$   $P_T$  at LO (blue) and NLO (gray) with  $\mu_F = \mu_R = m_T^{J/\psi}$ .

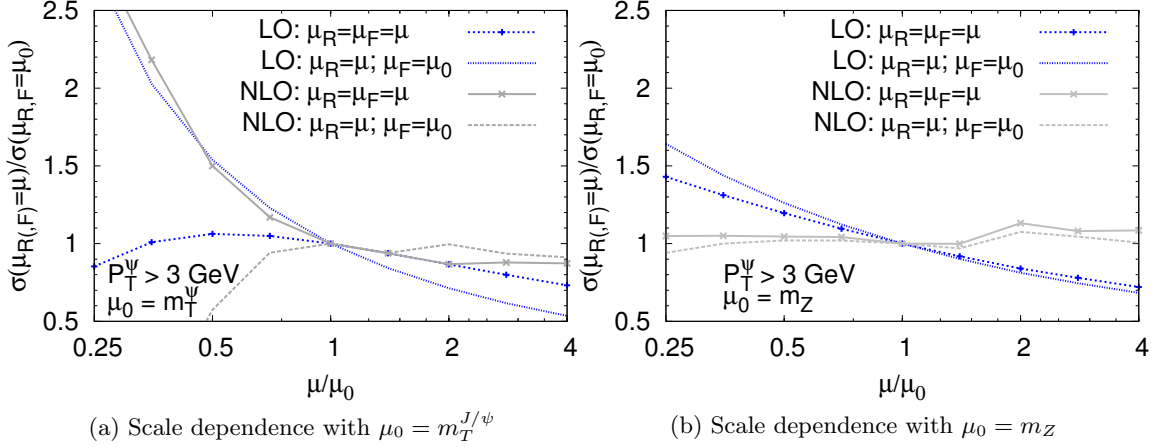


**Figure 3:** (a) Renormalisation and factorisation scale dependence of the LO and NLO yield for  $P_T > 3$  GeV with  $\mu_0 = m_T^{J/\psi}$ . (b) Same plot as (a) for  $\mu_0 = m_Z$ .

emphasise that we believe the latter choice to be more appropriate owing to the presence of the  $Z$  boson in the hard process. One sees that around  $m_Z$  (b), the cross section at NLO is more stable, except for the bump at  $2m_Z$  which can be corrected by properly setting the value of  $\Lambda^{[6]}$  in the running of coupling constant (currently 0.151 MeV with  $m_t = 180$  GeV), which matters for  $\mu_R > m_t$ . The NLO results are clearly unstable at low scales and they may then artificially be enhanced. In the following sections, we investigate further the dependence of the scale sensitivity for different domains of the  $J/\psi$  transverse momenta.



## 218 4.2 Results for the differential cross section in $P_T$ at $\sqrt{s} = 8$ TeV and 14 TeV

219 In the following, we show our results for  $|y^{J/\psi}| < 2.4$  –the usual  $J/\psi$  acceptance for the CMS  
 220 and ATLAS detectors– at 8 TeV and<sup>3</sup> 14 TeV and for the renormalisation and factorisation  
 221 scales set at  $m_Z$ . We have kept<sup>4</sup> the cut  $P_T^{J/\psi} > 3$  GeV.

222 The parameters entering the cross-section evaluation have been taken as follows:  $|R_{J/\psi}(0)|^2 =$   
 223  $0.91 \text{ GeV}^3$ ,  $\text{Br}(J/\psi \rightarrow \ell^+ \ell^-) = 0.0594$ ,  $m_c = 1.5 \text{ GeV}$  with  $m_{J/\psi} = 2m_c$ ,  $m_b = 4.75 \text{ GeV}$ ,  
 224  $\alpha = 1/128$ . Our result at  $\sqrt{s} = 14$  TeV are depicted on Fig. 4. The dotted blue line is our  
 225 LO result and the solid gray line is our prediction at NLO. It is obvious, contrary to what  
 226 was obtained in [32], that the yield at NLO is getting larger than at LO for increasing  
 227  $P_T$ . This is similar to what happens in the inclusive case. This is also indicative that new  
 228 leading  $P_T$  topologies, in particular  $t$ -CGE, start dominating rather early in  $P_T$  despite of  
 229 the presence of a  $Z$  boson in the process. At  $P_T = 150 \text{ GeV}$ , the NLO yield is already ten  
 230 times that of LO.

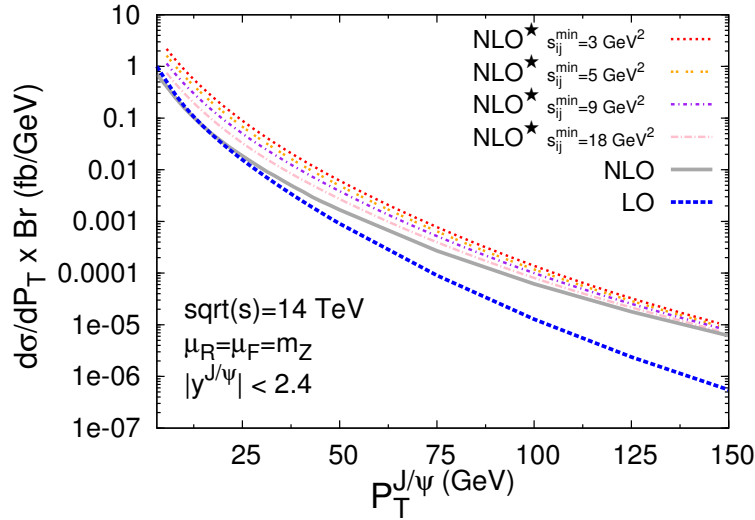


**Figure 4:** Differential cross section for  $J/\psi + Z$  vs.  $P_T$  at  $\sqrt{s} = 14$  TeV at LO (blue dashed) and NLO (gray solid) with  $\mu_F = \mu_R = m_Z$  along with the NLO\* for different values of  $s_{ij}^{\min}$  (red dotted, yellow double dotted, purple dash dotted and pink long-dash dotted).

231 The dominance of  $t$ -CGE topologies can be quantified by a comparison with the results  
 232 from the NLO\* evaluation. As aforementioned, because of the  $Z$  boson mass, it was not a  
 233 priori clear that the NLO\* evaluation could make any sense here. Indeed, as long as the  
 234 contribution from the sub-leading  $P_T$  topologies are significant, the NLO\* would strongly

<sup>3</sup>The cross section at 13 TeV is 12 % smaller than at 14 TeV.

<sup>4</sup>Note that we could have evaluated the cross section for lower  $P_T$  where the cross section is well behaved. However, we do not expect –at least in the central region– any experimental measurement to be carried out in this region owing to the momentum cut on the muons because of the strong magnetic fields in the ATLAS and CMS detectors.

depend on the arbitrary IR cutoff<sup>5</sup> which is used to mimic the effect of the loop contributions which regulate the soft gluon emission divergences. We are in a position to check from which  $P_T$  the NLO\* starts to reproduce the full NLO and becomes to be less sensitive on the IR cut.

The various dotted lines on Fig. 4 show the NLO\* evaluation for different cut-off values. Two observations can be made: 1) they converge to the NLO steadily for increasing  $P_T$ , 2) for  $P_T > m_Z$ , the NLO\* evaluations are within a factor of 2 compatible with the complete NLO yield. This confirms that loop corrections are sub-leading in  $P_T$  and can be safely neglected for  $P_T$  larger than all the masses relevant for the process under consideration and that new topologies appearing at NLO, the  $t$ -CGE ones, dominate at large  $P_T$ . At low  $P_T$ , where the NLO and LO yield are similar, the NLO\* overestimate the NLO.

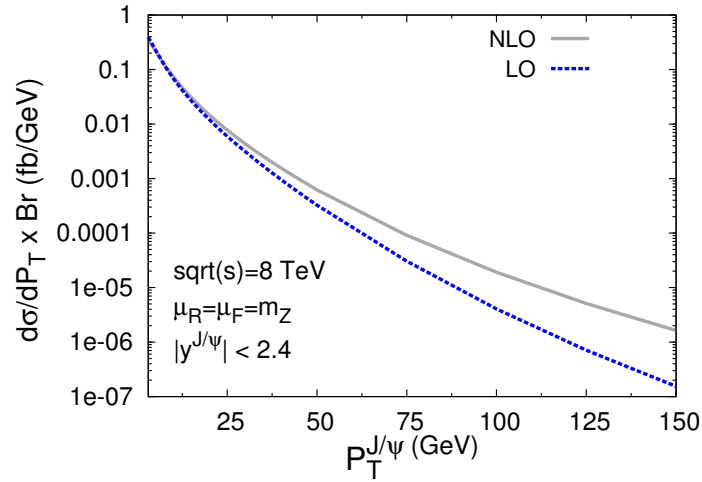


**Figure 5:** Differential cross section for  $J/\psi + Z$  vs.  $P_T$  at  $\sqrt{s} = 8$  TeV at LO (blue dashed) and NLO (gray solid) with  $\mu_F = \mu_R = m_Z$ .

As regards the possibility to study such a process at the LHC, the  $P_T$  differential cross sections times the branching  $\text{Br}(J/\psi \rightarrow \mu^+ \mu^-)$  at the smallest  $P_T$  accessible by ATLAS and CMS (3 to 5 GeV depending on the rapidity) is of the order of 1 fb/GeV at 14 TeV (Fig. 4) and three times less at 8 TeV (Fig. 5). These do not take into account the branching of the  $Z$  in dimuons ( $\sim 3\%$ ), but these are central values which can be affected by a factor of 2-3 of theoretical uncertainties. In the most optimistic case, by integrating on the accessible  $P_T$  range, by using both muon and electron decay channels for the  $J/\psi$ , by expecting an indirect cross section of 40 % and by detecting the  $Z$  boson with hadronic channels such that it could be detected 40 % of the time, it may be envisioned to detect something like four hundred events at 14 TeV with  $100 \text{ fb}^{-1}$  of data –possibly a factor 2-3 above given the theory uncertainty. At 8 TeV with the  $20 \text{ fb}^{-1}$  of data expected to be collected in 2012, we expect only about thirty events to be recorded. Clearly, there are more promising processes, such as  $J/\psi + \gamma$  [13, 14] or  $J/\psi + D$  [17, 41], to learn more on the production

<sup>5</sup>Not to be confused with the cutoff used in the full NLO computation, on which the final results does not depend.

mechanisms of the  $J/\psi$ . Nevertheless, the study of  $J/\psi + Z$  may suffer less from trigger limitations and could thus still be at reach at the LHC. In any case, it is an ideal theory playground to analyse the effects of QCD corrections on quarkonium production, which have been the key subject in the recent years in the field.

### 4.3 Scale sensitivity at different $P_T$

From the observations made above, we expect the real emission contributions at  $\alpha\alpha_s^3$  to dominate for  $P_T \gtrsim m_Z/2$ . This should therefore impact on the scale dependence of the yield. At low  $P_T$  ( $\ll m_Z$ ), we expect a reduced scale dependence since we really deal with a process at NLO accuracy. At large  $P_T$ , the leading process is  $pp \rightarrow J/\psi + Z + \text{parton}$ . The loop contributions are not expected to reduce the scale sensitivity since they are small. On the contrary, we expect a larger sensitivity on the renormalisation scale,  $\mu_R$ , since the leading process shows an additional power of  $\alpha_s(\mu_R)$ . In practice, we study the scale sensitivity by varying  $\mu_F$  and  $\mu_R$  together and then  $\mu_R$  alone by a factor 2 about the “default” scale  $m_Z$  with 3 cuts in  $P_T$  –i.e. 3, 50 and 150 GeV.

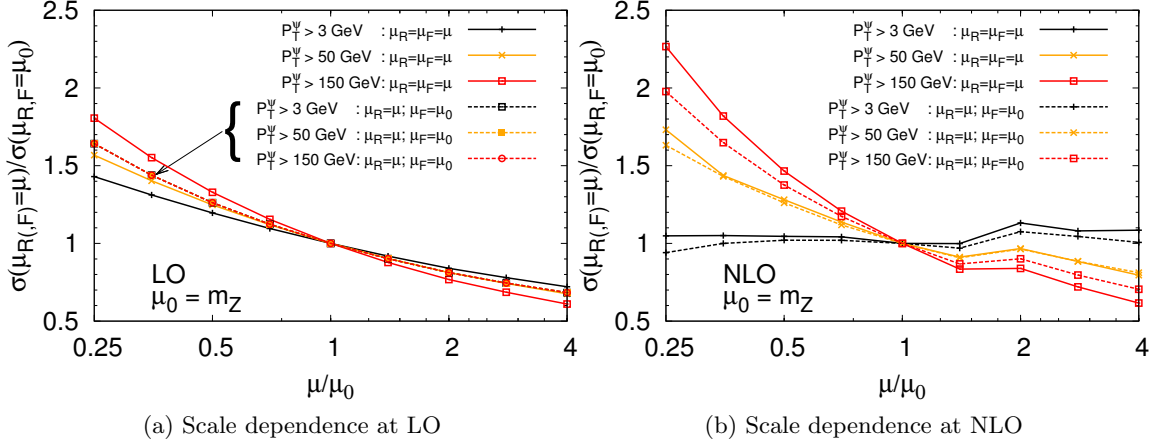


**Figure 6:** Scale dependence of the yield at LO (a) and NLO (b) for  $P_T > 3$  GeV,  $P_T > 50$  GeV,  $P_T > 150$  GeV where both the renormalisation and factorisation scales are varied together ( $\mu_F = \mu_R$ , solid lines) about  $\mu_0 = m_Z$  and only the renormalisation scale is varied ( $\mu_F$  fixed, dashed lines). Note that  $\alpha$  has been kept fixed.

On Fig. 6, we do observe, as anticipated for  $P_T \gtrsim m_Z$  (red curves), a stronger scale sensitivity of the NLO yield (b) –at  $\alpha\alpha_s^3$ – than of the LO yields (a)– at  $\alpha\alpha_s^2$ . The NLO curve with  $\mu_F$  fixed clearly shows that the sensitivity essentially comes from  $\mu_R$ . At mid  $P_T$  (orange curves), the scale sensitivities are similar at LO and NLO, while at low  $P_T$  (black curves), the NLO yield is less scale dependent than the LO –in agreement with the common wisdom regarding the NLO computations. Note also that the 3 LO curves showing the sole dependence of  $\mu_R$  are identical since one can factor out a common  $\alpha_s^2$  since our choices of  $\mu_R$  do not depend on  $P_T$ .

## 281 5 Polarisation: polar anisotropy in the helicity frame

282 The polar anisotropy of the dilepton decay of the  $J/\psi$ ,  $\lambda_\theta$  or  $\alpha$ , can be evaluated from the  
 283 polarised hadronic cross sections:

$$\alpha(P_T) = \frac{\frac{d\sigma_T}{dP_T} - 2\frac{d\sigma_L}{dP_T}}{\frac{d\sigma_T}{dP_T} + 2\frac{d\sigma_L}{dP_T}}. \quad (5.1)$$

284 To evaluate  $\alpha(P_T)$ , the polarisation of  $J/\psi$  must of course be kept throughout the  
 285 calculation. The partonic differential cross section for a polarised  $J/\psi$  is expressed as:

$$\frac{d\hat{\sigma}_\lambda}{d\hat{t}} = a \epsilon(\lambda) \cdot \epsilon^*(\lambda) + \sum_{i,j=1,2} a_{ij} p_i \cdot \epsilon(\lambda) p_j \cdot \epsilon^*(\lambda), \quad (5.2)$$

286 where  $\lambda = T_1, T_2, L$ .  $\epsilon(T_1)$ ,  $\epsilon(T_2)$ ,  $\epsilon(L)$  are respectively the two transverse and the longi-  
 287 tudinal polarisation vectors of  $J/\psi$ ; the polarisations of all the other particles are summed  
 288 over in  $n$  dimensions. One can find that  $a$  and  $a_{ij}$  are finite when the virtual and real  
 289 corrections are properly handled as aforementioned. There is therefore no difference in  
 290 the partonic differential cross section  $d\hat{\sigma}_\lambda/d\hat{t}$  whether the polarisation of  $J/\psi$  is summed  
 291 over in 4 or  $n$  dimensions. Thus, we can just treat the polarisation vectors of  $J/\psi$  in 4  
 292 dimensions. There are usually several different choices of the polarisation frames, as dis-  
 293 cussed in Ref. [42–44]. In our calculation, we have chosen to work in the helicity frame.  
 294 The polarisation can be obtained in a given frame by taking the corresponding polarisation  
 295 vectors in Eq. (5.2).

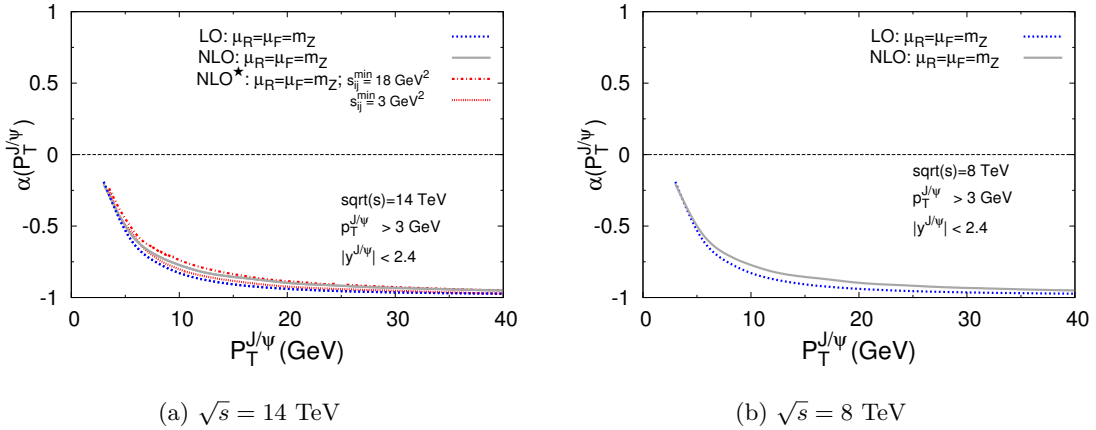


**Figure 7:** (a)  $P_T$  dependence of the polarisation (or azimuthal anisotropy) in the helicity frame of the direct  $J/\psi$  produced with a  $Z$  boson at LO, NLO and NLO\* (for 2 values of the IR cut-off) at  $\sqrt{s} = 14$  TeV. (b) Same as (a) at LO and NLO at  $\sqrt{s} = 8$  TeV.

296 Our results at 14 TeV in Fig. 7 (a) clearly show that the direct- $J/\psi$  yield in association  
 297 with a  $Z$  boson is increasingly longitudinally polarised in the helicity frame for increasing  
 298  $P_T^{J/\psi}$ . The NLO and NLO\* results coincide and the latter is nearly insensitive to the

IR cutoff. Interestingly, the NLO and the LO results are also very similar. This is the first time that such a robustness of the polarisation against QCD corrections is observed for the colour-singlet channels. For the  $J/\psi$  produced inclusively or in association with a photon, the yield at LO and NLO are found to have a completely different polarisation. Our interpretation is that, when a  $Z$  boson is emitted by one of the charm quarks forming the  $J/\psi$ , the latter is longitudinally polarised, irrespective of the off-shellness and of the transverse momentum of the gluons producing the charm-quark pair. This is not so when a photon or a gluon is emitted in the final state. In the present case, we also note that the polarisation at 8 TeV (Fig. 7 (b)) is nearly exactly the same as at 14 TeV.

## 6 Results for $\Upsilon + Z$

Along the same lines as for  $J/\psi$ , we have also evaluated the cross section and the polarisation for direct- $\Upsilon$  production in association with a  $Z$  boson. Experimentally, the CDF Collaboration at Fermilab has set a 95 % C.L. upper value for such a cross section at  $\sqrt{s} = 1.8$  TeV [45], namely

$$\sigma(p\bar{p} \rightarrow \Upsilon + Z + X) \times \text{Br}(\Upsilon \rightarrow \mu^+ \mu^-) < 2.5 \text{ pb.} \quad (6.1)$$

Further studies with the entire data set recorded by CDF is under process [46]. At  $\sqrt{s} = 1.8$  TeV, a quick evaluation of the total cross section (without  $y$  cut, nor  $P_T$  cut) gives, for the CSM, a value close<sup>6</sup> to 0.1 fb ( $\sim 0.2$  fb by taking into account a similar feed-down fraction ( $\sim 50\%$ ) than that for the inclusive case). A similar evaluation for the CO transitions is highly dependent on the choosen LDME values and on the expected impact of the feed-down. Values span from  $\sim 0.06$  fb for the direct yield with CO LDMEs fit [47] from the early prompt Tevatron data, up to  $\sim 3.75$  fb as evaluated in [48], passing by  $\sim 0.4$  fb for the direct yield using CO LDMEs fit from the latest Tevatron results taking into account some NLO QCD corrections [49].

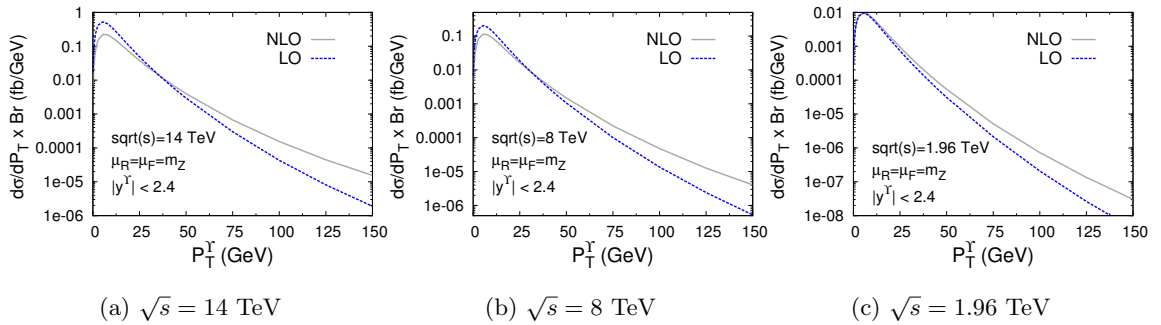


**Figure 8:** Differential cross section for direct  $\Upsilon + Z$  vs.  $P_T$  at LO (blue-dashed) and NLO (gray-solid) with  $\mu_F = \mu_R = m_Z$  at 14 TeV (a), 8 TeV (b) and<sup>7</sup> 1.96 TeV (c).

<sup>6</sup>We should however keep in mind that these are central values and that theoretical uncertainties can be of the order of a factor 2-3.

322 This, is in any case, significantly below the CDF upper bound obtained with  $83 \text{ pb}^{-1}$   
 323 of data. Given these small theoretical values, we fear that such process cannot be experi-  
 324 mentally accessed at the Tevatron, unless contributions from colour-octet transitions, from  
 325 double-parton interactions or from feed-downs are unexpectedly large. At the LHC at 14  
 326 TeV, the expected yield in the CSM for the central rapidity region accessible by CMS and  
 327 ATLAS is of the order 5 fb (still including the branching of the  $\Upsilon$  in muons). The central  
 328 values for the differential cross sections vs.  $P_T$  at LO and NLO are shown in Fig. 8 (a-c).  
 329 An enhancement by a factor 2 to 4 can certainly be expected if the feed-downs from excited  
 330 bottomonium states and the usual theoretical uncertainties are taken into account.

331 By comparing Fig. 8 (a-c), one also notices an interesting phenomenon: the NLO and  
 332 LO yields start to depart from each other at low  $P_T$  for increasing  $\sqrt{s}$ . This can probably  
 333 be attributed to an increasing –negative– size of the loop corrections in this region at small  
 334  $x$ . This is in fact reminiscent to what has been observed in the inclusive case [4, 6, 17, 18].  
 335 In the latter case, the situation is worse since the NLO cross section can become negative  
 336 for large  $\sqrt{s}$  and small  $P_T$ . It hints at significant NNLO corrections at small  $P_T$  in the  
 337 small- $x$  region, as anticipated in [50].

338 For the sake of the comparison with the  $J/\psi$  case, we have also computed the polari-  
 339 sation at LO and NLO. As it can be seen on Fig. 9, the yield polarisation at LO and NLO  
 340 are very alike, though slightly different from for the  $J/\psi$  case –most probably due to the  
 341 change in the quarkonium mass compared to the  $Z$  mass.

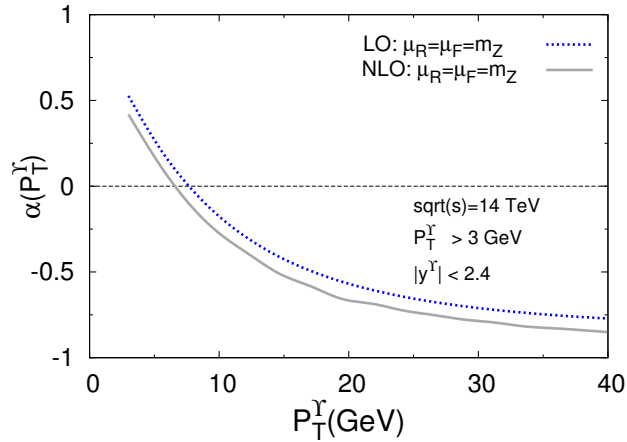


**Figure 9:**  $P_T$  dependence of the polarisation (or azimuthal anisotropy) in the helicity frame of the direct  $\Upsilon$  produced with a  $Z$  boson at LO and NLO at  $\sqrt{s} = 14 \text{ TeV}$ .

<sup>7</sup>We have considered a wider rapidity range than usual for the CDF quarkonium analyses since CMX muons can be used in such a correlation analysis owing to the smaller background compared to inclusive measurements [46].

## 7 Conclusions

In conclusion, we have studied the effects of the QCD corrections to the production of direct  $J/\psi$  and  $\Upsilon$  via colour-singlet transitions in association with a  $Z$  boson at the LHC. We have found, contrary to an earlier study [32], that the NLO QCD corrections are consistent with the expectations, namely increasing for increasing  $P_T$  and small at low  $P_T$ . We expect that a few hundred  $J/\psi + Z$  events could be detected at the LHC at 14 TeV with  $100 \text{ fb}^{-1}$  of data. At 8 TeV with  $20 \text{ fb}^{-1}$ , there may be just enough events to derive a cross section and not only an upper bound on its value. Interestingly, the CSM yield expected for direct  $\Upsilon + Z$  is of the same order of magnitude than that of direct  $J/\psi + Z$  at 14 TeV, if not larger.

We have studied the scale sensitivity of the  $J/\psi + Z$  cross section at LO and NLO. At low  $P_T$ , it is smaller when QCD corrections are taken into account. On the contrary, at large  $P_T$ , *i.e.* when  $P_T \gtrsim m_Z/2$ , the dominant contributions are of the kind of  $gg \rightarrow Q + Z + \text{jet}$ . These involve an additional power of  $\alpha_s$  and the sensitivity on the renormalisation scale is larger. Along the same lines of arguments, one expects a further increase of the CSM cross section at large  $P_T$  when the leading- $P_T$  contribution contained in the NNLO topologies are accounted for. That being said, the presence of the  $Z$  boson mass renders the CSM prediction more precise at low  $P_T$  compared to the inclusive case, for which the leading- $P_T$  contributions at NLO and NNLO dominate at lower  $P_T$ .

We have also found that the yield polarisation is not altered by the QCD corrections. From this observation, we have concluded that when a  $Z$  boson is emitted by one of the heavy quarks forming the quarkonium, both the  $J/\psi$  and the  $\Upsilon$  are longitudinally polarised at LO and NLO, thus independently of the off-shellness and of the transverse momentum of the gluons producing the heavy-quark pair. This is at odds with the cases of inclusive  $Q$  production and  $Q + \gamma$  production, and this motivates further theoretical and experimental investigations.

## Acknowledgements

This work is supported in part by the France-China Particle Physics Laboratory, by the P2I network and by the National Natural Science Foundation of China (Nos. 10979056 and 11005137).

## References

- [1] M. Kramer, Prog. Part. Nucl. Phys. **47**, 141 (2001) [hep-ph/0106120].
- [2] N. Brambilla *et al.*, CERN Yellow Report 2005-005, hep-ph/0412158
- [3] J. P. Lansberg, Int. J. Mod. Phys. A **21**, 3857 (2006) [hep-ph/0602091].
- [4] J. Campbell, F. Maltoni and F. Tramontano, Phys. Rev. Lett. **98**, 252002 (2007) [hep-ph/0703113].
- [5] P. Artoisenet, J. P. Lansberg and F. Maltoni, Phys. Lett. B **653**, 60 (2007) [hep-ph/0703129].
- [6] B. Gong and J. X. Wang, Phys. Rev. Lett. **100** (2008) 232001. [arXiv:0802.3727 [hep-ph]];

- [7] B. Gong and J. X. Wang, Phys. Rev. D **78** (2008) 074011. [arXiv:0805.2469 [hep-ph]].
- [8] P. Artoisenet, J. Campbell, J. P. Lansberg, F. Maltoni and F. Tramontano, Phys. Rev. Lett. **101** (2008) 152001. [0806.3282 [hep-ph]].
- [9] C-H. Chang, Nucl. Phys. B **172** (1980) 425; R. Baier and R. Rückl, Phys. Lett. B **102** (1981) 364; R. Baier and R. Rückl, Z. Phys. C **19** (1983) 251.
- [10] J. P. Lansberg, Eur. Phys. J. C **61** (2009) 693 [arXiv:0811.4005 [hep-ph]].
- [11] N. Brambilla, *et al.* Eur. Phys. J. C **71** (2011) 1534 [arXiv:1010.5827 [hep-ph]].
- [12] Z. Conesa del Valle, G. Corcella, F. Fleuret, E. G. Ferreira, V. Kartvelishvili, B. Kopeliovich, J. P. Lansberg and C. Lourenco *et al.*, Nucl. Phys. (PS) **214** (2011) 3 [arXiv:1105.4545 [hep-ph]].
- [13] R. Li and J. X. Wang, Phys. Lett. B **672** (2009) 51. [arXiv:0811.0963 [hep-ph]].
- [14] J. P. Lansberg, Phys. Lett. B **679** (2009) 340. [arXiv:0901.4777 [hep-ph]].
- [15] A. K. Leibovich, Phys. Rev. D **56** (1997) 4412 [hep-ph/9610381].
- [16] C. S. Kim and E. Mirkes, Phys. Rev. D **51** (1995) 3340 [hep-ph/9407318].
- [17] S. J. Brodsky and J. P. Lansberg, Phys. Rev. D **81** 051502(R) (2010). [arXiv:0908.0754 [hep-ph]].
- [18] J. P. Lansberg, PoS ICHEP **2010** (2010) 206 [arXiv:1012.2815 [hep-ph]].
- [19] J. P. Lansberg, to appear in Nucl. Phys. A. [arXiv:1209.0331 [hep-ph]].
- [20] A. Adare *et al.*, Phys. Rev. Lett. **98** 232002 (2007) . [arXiv:hep-ex/0611020].
- [21] B. I. Abelev *et al.* [STAR Coll.], Phys. Rev. D **82** (2010) 012004 [arXiv:1001.2745 [nucl-ex]].
- [22] D. E. Acosta *et al.* [CDF Coll.], Phys. Rev. Lett. **88**, 161802 (2002).
- [23] V. M. Abazov *et al.* [D0 Coll.], Phys. Rev. Lett. **94**, 232001 (2005) [Erratum-ibid. **100**, 049902 (2008)] [hep-ex/0502030].
- [24] V. Khachatryan *et al.* [CMS Coll.], Phys. Rev. D **83** (2011) 112004 [arXiv:1012.5545 [hep-ex]].
- [25] G. Aad *et al.* [ATLAS Coll.], Phys. Lett. B **705** (2011) 9 [arXiv:1106.5325 [hep-ex]].
- [26] R. Aaij, *et al.* [The LHCb Coll.], Eur. Phys. J. C **72** (2012) 2025 [arXiv:1202.6579 [hep-ex]].
- [27] R. Aaij *et al.* [LHCb Coll.], Eur. Phys. J. C **71** (2011) 1645 [arXiv:1103.0423 [hep-ex]].
- [28] K. Aamodt *et al.* [ALICE Coll.], Phys. Lett. B **704** (2011) 442 [arXiv:1105.0380 [hep-ex]].
- [29] F. Cooper, M. X. Liu and G. C. Nayak, Phys. Rev. Lett. **93** (2004) 171801 [hep-ph/0402219].
- [30] Z. G. He, Y. Fan and K. T. Chao, Phys. Rev. D **81** (2010) 054036. [arXiv:0910.3636 [hep-ph]]. Y. J. Zhang, Y. Q. Ma, K. Wang and K. T. Chao, Phys. Rev. D **81** (2010) 034015. [arXiv:0911.2166 [hep-ph]]. Y. Q. Ma, Y. J. Zhang and K. T. Chao, Phys. Rev. Lett. **102** (2009) 162002; [arXiv:0812.5106 [hep-ph]]. B. Gong and J. X. Wang, Phys. Rev. Lett. **102** (2009) 162003. [arXiv:0901.0117 [hep-ph]].
- [31] F. Maltoni, *et al.* Phys. Lett. B **638** (2006) 202 [hep-ph/0601203].
- [32] S. Mao, M. Wen-Gan, L. Gang, Z. Ren-You and G. Lei, JHEP **1102** (2011) 071 [arXiv:1102.0398 [hep-ph]].
- [33] B. Gong and J. -X. Wang, Phys. Rev. D **80** (2009) 054015 [arXiv:0904.1103 [hep-ph]].



- 419 [34] J. -X. Wang, Nucl. Instrum. Meth. A **534** (2004) 241 [hep-ph/0407058].
- 420 [35] G. Duplancic and B. Nizic, Eur. Phys. J. C **35** (2004) 105 [hep-ph/0303184].
- 421 [36] B. W. Harris and J. F. Owens, Phys. Rev. D **65** (2002) 094032 [hep-ph/0102128].
- 422 [37] G. Altarelli, R. K. Ellis and G. Martinelli, Nucl. Phys. B **157** (1979) 461.
- 423 [38] P. Artoisenet, F. Maltoni and T. Stelzer, JHEP **0802** (2008) 102. [0712.2770 [hep-ph]].
- 424 [39] MADONIA can be used online (model “Quarkonium production in SM”) at  
425 <http://madgraph.hep.uiuc.edu>.
- 426 [40] J. M. Campbell, R. K. Ellis, F. Maltoni and S. Willenbrock, Phys. Rev. D **69** (2004) 074021  
427 [hep-ph/0312024].
- 428 [41] LHCb Collaboration, JHEP **1206** (2012) 141 [arXiv:1205.0975 [hep-ex]].
- 429 [42] M. Beneke, M. Kramer and M. Vanttinen, Phys. Rev. D **57** (1998) 4258 [hep-ph/9709376].
- 430 [43] P. Faccioli, C. Lourenco, J. Seixas and H. K. Wohri, Eur. Phys. J. C **69** (2010) 657  
431 [arXiv:1006.2738 [hep-ph]].
- 432 [44] P. Faccioli, Mod. Phys. Lett. A **27** (2012) 1230022 [arXiv:1207.2050 [hep-ph]].
- 433 [45] D. Acosta *et al.* [CDF Collaboration], Phys. Rev. Lett. **90** (2003) 221803.
- 434 [46] M. Kruse, A. Limosani, C. Zhou, private communications.
- 435 [47] P. L. Cho and A. K. Leibovich, Phys. Rev. D **53** (1996) 6203 [hep-ph/9511315].
- 436 [48] E. Braaten, J. Lee and S. Fleming, Phys. Rev. D **60** (1999) 091501 [hep-ph/9812505].
- 437 [49] B. Gong, J. -X. Wang and H. -F. Zhang, Phys. Rev. D **83** (2011) 114021 [arXiv:1009.3839  
438 [hep-ph]].
- 439 [50] V. A. Khoze, A. D. Martin, M. G. Ryskin and W. J. Stirling, Eur. Phys. J. C **39** (2005) 163  
440 [hep-ph/0410020].